EUROFUSION WPJET1-CP(16) 15159

M Valisa et al.

The role of ELM's and inter-ELM phases in the transport of heavy impurities in JET

Preprint of Paper to be submitted for publication in
Proceedings of 26th IAEA Fusion Energy Conference

This work has been carried out within the framework of the EUROfusion Consortium and has received funding from the Euratom research and training programme 2014-2018 under grant agreement No 633053. The views and opinions expressed herein do not necessarily reflect those of the European Commission.

The role of ELM's and inter-ELM phases in the transport of heavy impurities in JET

M. Valisa[1], A. Loarte[10,] L. Amicucci[2], C. Angioni[3], R. Cesario[2], L. Carraro[1], D. Coster[3], F. J. Casson[4], I. Coffey[5], E. De la Luna[6], P. Devynk[7], P. Drewelow 8, L. Frassinetti [9], C. Giroud[4], F. Koechl[9], M. Leyland[4], I Lupelli[4], M. Marinucci[2], S. Menmuir[4], M. O'Mullane[11],V. Parail[4], A. Patel[4], M. E. Puiatti[1], E. Rachlew[9] , M.Romanelli[4], E. Stefanikova[9] and JET contributors*

EUROfusion Consortium, JET, Culham Science Centre, Abingdon, OX14 3DB, UK

[1] Consorzio RFX, Padova, Italy,

[2] ENEA Via E Fermi 45, 00044 Frascati RM, Italy

[3]Max Planck Institut für Plasmaphysik, Garching, Germany,

[4]CCFE, Culham Science Centre, Abingdon, OX14 3DB, UK,

[5]Queen's University, Belfast, UK

[6]Laboratorio Nacional de Fusión, CIEMAT, Madrid, 28040, Spain

[7]CEA-IRFM F-13108 Saint-Paul-lez-Durance, France

[8]Max-Planck Institut für Plasma Physik, 17491 Greifswald, Germany

[9]KTH, Royal Institute of Technology, Sweden

[10] ITER Organization, Route de Vinon sur Verdon, 13115 Saint Paul Lez Durance, France

[11]Department of Physics SUPA, University of Strathclyde, Glasgow, G4 ONG, UK

*See the Appendix of F. Romanelli et al., Proc. 25th IAEA FEC 2014, S Petersburg, Russia.

E-mail contact of main author: valisa@igi.cnr.it

Abstract. A series of dedicated experiments have started at JET in order to study in detail the way type 1 ELM's and intra-ELM periods determine the transport of heavy impurities at the edge of the plasma. For the purpose, trace amounts of extrinsic Mo, Kr and Ne have been injected in 10-12 MW NBI heated elmy H-mode discharges, and the evolution of their content in the plasma has been analyzed. Spontaneous ELM's have been compared with ELM's triggered by vertical kicks. The main results are: the ELM process reduces the content of all impurities regardless of their masses and the finding applies to W as well. Natural and kicks-induced ELM's behave similarly with respect to the impurity expulsion. Simulation of the impact of a single ELM on Mo injected via Laser Blow Off appears to be a good tool to investigate the nature of the ELM induced transport.

1. Introduction

This work has been primarily motivated by the concern that Edge Localized Modes (ELM) in ITER may increase W concentration compromising the plasma performance, reduce the plasma reactivity and undermine the stability of the discharge. The concentration of W in the plasma depends on the source and on the transport in the specific plasma scenario. W is mainly produced by erosion at the divertor both in the phases between ELM's and during ELM's. It first crosses the Scrape-Off-Layer, then the pedestal region, where it is periodically expelled by ELM's, and eventually spreads into the plasma core according to the local transport. In devices with W divertors such as JET and AUG [1], techniques have been developed to limit the W concentration within acceptable levels by optimizing core heating and ELM control [2,3]. ELM frequency can be extended beyond its natural level by adding fuelling gas or by pacing them by injecting pellets , inducing vertical displacements of the

plasma column (kicks) or also by applying resonant magnetic perturbations [3,4,5]. Such techniques affect all of the above mentioned transport phases simultaneously and make the drawing of quantitative conclusions about the relevance of each physics processes in the resulting W contamination of the core plasma difficult. Now, current understanding suggests that in the ITER baseline scenario W should not be an issue [3]. In the core of the plasma tungsten should not experience an important inward drive due to relatively mild electron density gradients, the absence of significant torque which would reinforce the neoclassical convection term and the expected decrease of the neoclassical to total heat flux ratio with increasing power and size [6]. At the edge, because of the dominance of the neoclassical temperature screening over the density gradient, which instead attracts W into the main plasma, W transport in-between ELM's can be very favourable leading to an outward flux of W and therefore to a hollow W density profile at the edge [7]. In such conditions, depending on the dominant mechanism for W expulsion by ELMs, whether convective or diffusive, ELMs could contribute to bring W impurity into the plasma rather than expelling it. Hence the interest in improving our understanding on the relative role of ELM an inter-ELM phases on imuity transport. Such topic has been subject of both experimental and theoretical investigations. In [8] time and space resolved density profile measurements of impurities from He to Ar have led to the determination of accurate impurity transport parameters in between ELM's in ASDEX Upgrade, which resulted to be essentially neoclassical, and to the development of a simplified integrated model of edge transport a impurity source. The transport during ELM's was represented as mainly diffusive, with null convection. In [9] time and space resolved impurity measurements in DIII-D showed that impurities and main density experience similar drops during the ELM, signature of a species independent action, and that the impurity energy transport during ELMs is dominated by convection. In [10] the interplay in JET of W sputtering, transport across the SOL and the edge barrier has been investigated to explain the accumulation of W. Broad experimental observations [11-15] show that the ELM crash is characterized by the growth of 3D filaments and filament holes which eventually leave radially the plasma with velocities of the order of several km/s and heat the walls, suggesting that the ELM induced losses are mainly convective. The complex physics involved during the ELM crash is nowadays tackled by means of 3D MHD codes, as for instance in [16] .

To further improve the understanding of the physics mechanisms that control the penetration of high Z impurities from the divertor into the core, traces of extrinsic impurities have been injected into ELMy H-mode JET plasmas. The use of extrinsic impurities avoids the need to deconvolve the impurity source. The W source at the divertor has in any case been monitored so as to extend the analysis to W too for comparison. In the following we show the results of the injection of Mo, Kr and Ne in 10-12 MW NBI heated 2.1 T/2 MA low triangularity discharges with spontaneous ELM's and ELM's triggered by vertical kicks and the initial analysis of the impact of ELM's on Mo injected via LBO.

2. Experiment and results

The plasma target selected for the experiment featured electron density and temperature profiles as those shown in Fig 1. Two sets of discharges have been generated, differing only for the input power of 12 and 10 MW of NBI respectively. In all cases the outer leg at the divertor was kept on the horizontal W tile, which intercepts the line of sight of visible spectrometers and where Langmuir probes measure the local electron temperature so that the W source could be monitored. The profiles shown in Fig. 1 represent conditioned averages, with samples selected in the phase between 60 and 90%. of the ELM cycle. The kinetic profiles are all very similar, with small variation of the density and the temperature due to the

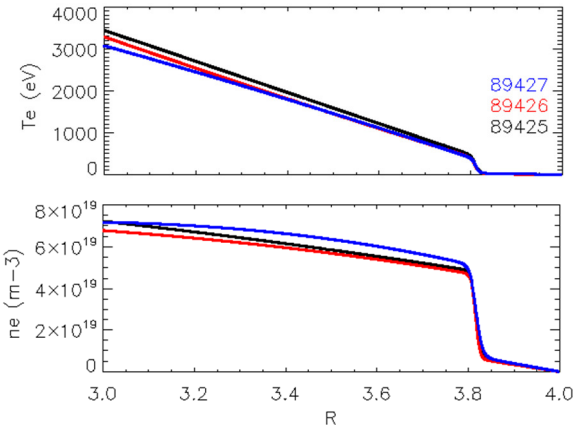

Fig. 1 T_e and n_e of the three discharges indicated in the top panel.

change in the gas rate from discharge to discharge. Increasing the gas rate was in fact one of the methods utilized to increase the ELM frequency, the second one being the application of vertical kicks with the desired frequency. The way kicks are applied at JET may be found in details in [4]. Table 1 summarises the collected database in terms of gas fuelling rate, ELM frequencies, injected impurities and input power. Mo was injected in all of the discharges by means of Laser Blow Off 1 second after the beginning of the NBI power, while a valve on the equatorial plane injected gaseous impurities later in the flattop; neon in the first set of discharges and kripton in the second one. The valve was opened each time for 100 ms in order to be able to follow the complete evolution of the impurities getting in and out of the plasma. Precise characteristic times of the gas injections can be evaluated by means of fast baratrons measuring the pressure inside the vessel after injections in vacuum, but such an exercise has not been carried out as yet. Spectroscopic signals tell us anyway that such characteristic times are of the order of seconds, while the injection of impurities via LBO is exhausted in a time that in JET is estimated around 10 ms. The ELM frequency in the database changes by a factor 2.5 at most and the amplitude of the ELMs themselves does not change significantly as it is shown in Fig. 2. In these discharges the energy loss per ELM is of the order of 0.2 MJ. Nevertheless, we will see in the following how such relatively small changes are sufficient to introduce sizeable differences in the impurity concentrations. The results of injecting impurities are summarized in Figures 3 to 5. Fig. 3 shows as a function of time the intensity of the Kr XXVI (17.89 nm) emission line normalized to the electron density, which represents a quantity proportional to the Kr density. According to transport simulations in which the turbulent transport has been assumed the one suitable for Mo (see below), such Kr line emission, chord integrated by a VUV spectrometer with a horizontal LOS, is from an ionization stage that populates a large region of the plasma

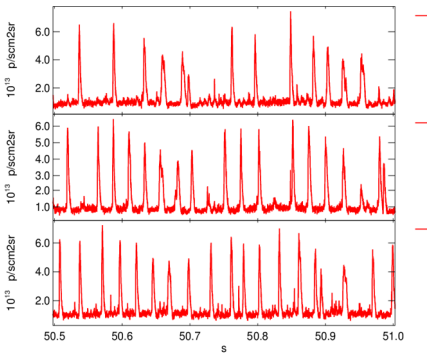

Fig. 2 Example of ELM sequences for the discharges from 89425 (top) to 89427 (bottom).

Table 1: the database

#	Gas rate1e22 e/s	Elm freq. (Hz)	Impurity	Kicks	NBI (MW)
89425	0.82	25	Mo, Ne		12.5
89426	0.87	36	Mo, Ne	Yes	12.5
89427	1.58	35	Mo, Ne		12.5
90606	0.84	20	Mo		10
90607	0.84	22	Kr	Yes	10
90608	0.81	41	Mo, Kr	Yes	10
90609	1.26	37	Mo, Kr		10
90610	1.94	52	Mo, Kr		

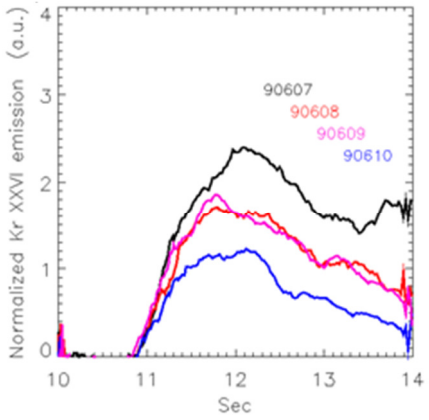

Fig.3. Kr XXVI line emission normalized to the electron density following the injection at 10.5 s.

with a peak around 0.9 of the normalized radius and that extends wide into the core. Kr is puffed at 10.5 sec and is seen on the spectrometer after 400 ms. Signal amplitude and ELM frequencies are opposite to each other. Discharge 90607 has the lowest gas rate, the lowest ELM frequency and the highest Kr density in the plasma. The two discharges 90608 and 90609 have approximately the same ELM frequency and same signal amplitude. 90608 has the fuelling rate identical to that of 90607 but a higher ELM frequency, paced by kicks. In 90609 instead, kicks have been removed and the gas rate has been raised to match the ELM frequency of 90608. The fourth discharge, 90610 has the highest gas rate and ELM frequency and the lowest signal amplitude. When comparing these results we assume that the Kr inflow was the same for all of the discharges. However further investigations are needed to tell if the chosen configuration, in which pumping at the divertor is not optimized, may for instance explain the signal recovery that occurs at a certain point in each of the traces of Fig,1 and the fact that in the decay phase the traces are approximately parallel while they split significantly in the penetration phase.

Fig. 4 shows the time waveforms of the neon density at mid-radius and at 0.9 as measured by the CXRS systems for three discharges. Ne is injected at 12.3 sec and shows up in the spectrometer about 200 ms after. Unlike the Kr case, here the measurements are local. A Ne VIII emission line, representative of the Ne density immediately inside the separatrix, does not show any difference among the three discharges, meaning that the Ne influx is indeed quite comparable. As for Kr, the Ne density in the plasma decreases with the ELM frequency. With respect to discharge #89425, in #89426 the ELM frequency was increased by means of vertical kicks and then in 89427, without kicks, the puffing rate was topped up to match the ELM frequency of #89426. For the latter two discharges with similar ELM frequencies the Ne densities do not overlap as well as in the Kr case but remain close one to each other, certainly within the error bars, and clearly separated from the low ELM frequency case.

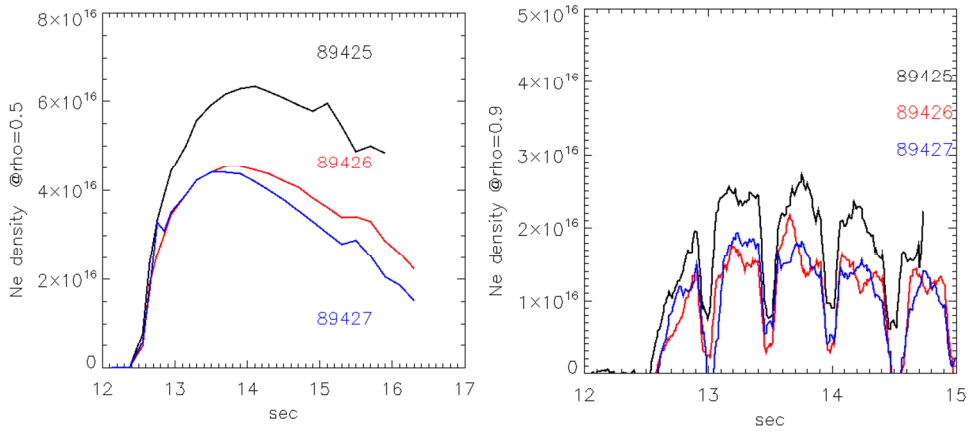

Fig.4. Ne density following injection at 12.3 sec from CXRS at mid radius (left) and at 0.9 of the normalized radius (right) as a function of time.

The injection of Mo by means of the LBO was at 49.5 s. In Fig. 5 we have plotted the waveforms of the Mo XXXII emission line seen by the VUV spectrometer, normalized to the

electron density. In the examined discharges, the monitored Mo state features a density that peaks around rho = 0.4 and extends to the centre of the plasma. Unlike the cases of Ne and Kr here the signal level does not depend on the ELM frequency. This is due to various reasons. The whole evolution of Mo is much faster than for Ne and Kr, whose influxes last much longer. Therefore any effects of the ELM's or of the inter-ELM processes are amplified in the latter cases with respect to Mo. Besides the poor sensitivity of the spectrometer for the given signal level, which smears out details in each discharge, the monitored Mo state populates the centre of the plasma and therefore within the typical transport time scale is not expected to be sensitive to a small number of events that may occur at the edge. This may be clarified by looking at the SXR where the differences among the discharges on the external channels vanish on the inner ones. In Fig.6, for instance, channel 28 of the vertical SXR camera, with an impact parameter of about 0.7, is compared to channel 20, with an impact parameter of 0.4, for the three discharges of Fig. 5. The time traces are well separated on the external channel (top panel) but overlap on the inner ones.

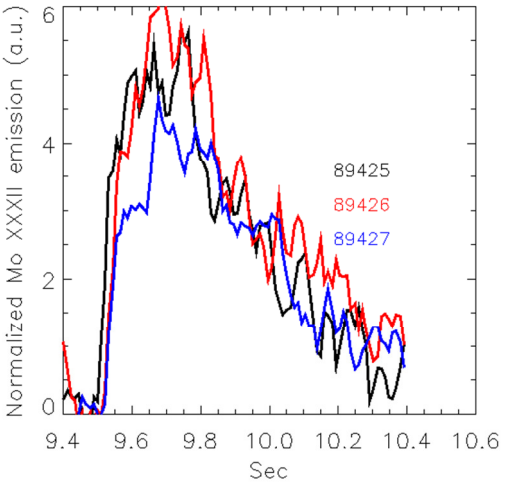

Fig. 5. Time waveforms of MoXXXII for the 3 discharges indicated in the panel. Mo isinjected via LBO at 9.5 s

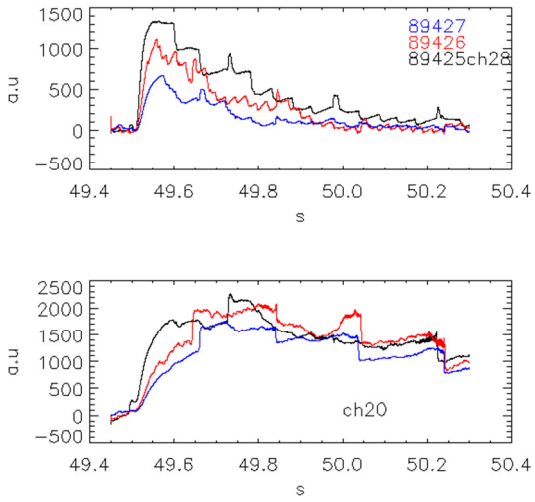

Fig. 6 The Mo LBO seen on the time traces of the SXR emission for two channels of the vertical camera and for the three discharges indicated in the top panel . The top panel refers to a "peripheral" position.

One may nonetheless note that in Fig 6 the way Mo penetrates the plasma in the three discharges is different, being faster for 89425 than for the other two cases, particularly for 89427. Since in all of the three examined cases there are no ELMs at the time of the injection, the latter difference must be due to transport effects. These are only qualitative considerations and a proper transport analysis is required to be more precise. For the above discharges we have compared the level of W concentration and the ELM frequencies taking into account the variation of the W source. To evaluate the W concentration in the various discharges we have analysed the level of energy integrated SXR emission, subtracted the contribution of the hydrogenic species to continuum radiation and assumed that W is the dominant impurity species amongst the metals present in the JET plasmas [17].

To corroborate such an assumption the results have been checked against the level of the W XLIII line emission recorded by the Bragg crystal spectrometer. The W source has been instead evaluated from the 400.1 nm W I line emitted at the divertor, taking into account the electron temperature measured locally by the Langmuir probes and the inverse photon efficiency as reported in [18]. In the latter exercise, however, the effects of the ELM

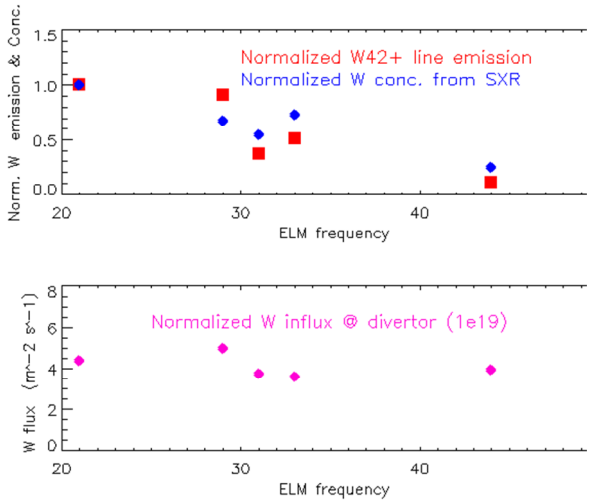

Fig. 7. Normalized emission of W42+ (top left) , W concentration (top right) and estimated W influx at the divertor(right) for the discharges indicated in the figures

themselves have not been fully included as the plasma temperature at the peak of the ELM process was not available. Fig. 7 summarizes the dependence of the W content as a function of the ELM frequency for the second group of discharges (90606 to 90610). The concentration of W decreases as the ELM frequency increases, while the source does not evidence important trends. Normalized W line emission and estimated W concentration appear to decrease by the same factor as the ELM frequency changes. The W content increases by a factor 4 against an increase of a factor 2 of the ELM frequency. This is similar to the drop of more than a factor 2 of the Kr content for a 50% increase of the ELM frequency.

3. Simulation of single ELM impact on injected Molybdenum

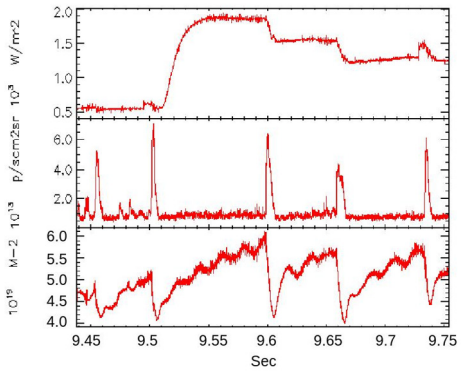

Fig. 8. Drop of (top) an SXR peripheral vertical channel and of (bottom) an outer vertical interferometer chord associated to ELM events (centre) during an LBO of Mo starting is at 9.5 sec. in discharge 89425.

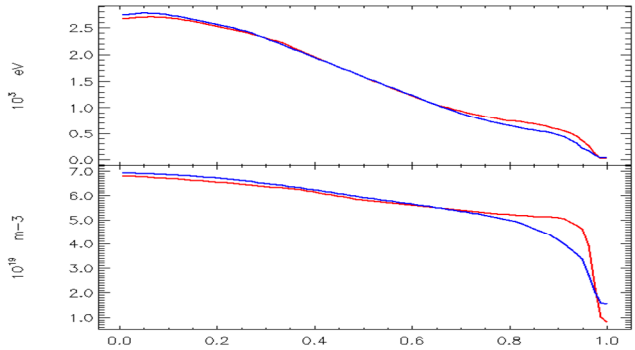

Fig. 9 . Te (top) and ne(bottom) profiles soon before (red) and after (blue) the ELM crash showing how the ELM affects the plasma up to around rho =0.7

Following Mo injection via LBO, clear effects of the ELMs are visible on several outer channels of the SXR cameras. These signatures can be used to analyze in detail the impact of a single ELM event on the Mo density, compute how much material is expelled and the depth into the plasma that an ELM can affect. In principle, given the transient nature of the process one should be able to disentangle the convective and the diffusive components of the involved transport, assuming that transport can be described in that way. In Fig .8 the time trace of channel 28 of the vertical camera is plotted together with the Be emission signal at the divertor, showing the ELM events, and the corresponding drop of the fast bolometer, indicating the drop of the line integrated density on a peripheral outer chord. It is worthwhile noting that the important drops induced by the ELMs are visible on the SXR signal only after the LBO is fired. In other words, in these circumstances of moderate input power, there is no need to disentangle the

signal due to Mo from the evolution of the background, dominated by W radiation. A preliminary analysis of the drop in the SXR emission has been carried out by means of the JETTO/SANCO transport code [19]. Here JETTO is used in interpretive mode. The evolution of the background kinetic profiles in an ELM cycle is given in input. Te, ne , Ti and rotation profiles in the ELM cycle have been statistically evaluated by ordering the profiles according to the time of their occurrence after an ELM crash. SANCO is instead predictive. The impurity transport is neoclassical (NCLASS) plus a diffusive component that is adjusted in such a way that the experimental perturbation of the SXR profile due to the LBO is grossly matched in the simulation. SANCO's grid protrudes into the SOL by several centimetres at the end of which particles are lost as recycling of Mo is set to zero. A properly adjusted constant inflow of Mo assures that an equilibrium Mo density is reached. The LBO injection is represented by a strong inflow with a 1 ms raise time and 5 ms decay time followed by a residual tail of 4 ms. First, a simulation of the Mo LBO is carried out by analysing only the effect of the evolution of the kinetic background, which is the drop of density and temperature profiles at the edge shown in Fig. 9 and the following recovery as seen in the experiment, neglecting any transport changes during the ELM itself. The change in transport following the change in temperature and density profiles is assumed to modify only the neoclassical components. With this assumption the impact of the ELM on the LBO evolution is almost negligible. Fig. 10 shows the diffusive and convective transport parameters used in the simulation and the time evolution of the Mo density at about mid radius following the LBO at 51.1 sec. More pronounced wiggles are seen in the reconstructed SXR's chords, mainly due to the different rate at which temperature and density recover after the ELM crash (see Fig. 11). Then the simulation of the ELM crash is introduced. To do so the crash is represented by 1) a large increase of the outward convection from the edge to the top of the pedestal (magenta traces in Fig 10) 2) a large increase of the outward convection that from the edge extends to about rho~ 0.7 (black) 3) a large increase of the diffusive component at the edge barrier (blue). Note that in Fig 10 the enhanced transport parameters are divided by 10. It appears that cases in which diffusion has been increased to simulate the ELM crash are less efficient in producing the drop in the Mo density than those cases in which convection has been increased. Extending further inside the plasma the increase of the transport parameters, either *v* or D, as in the case of

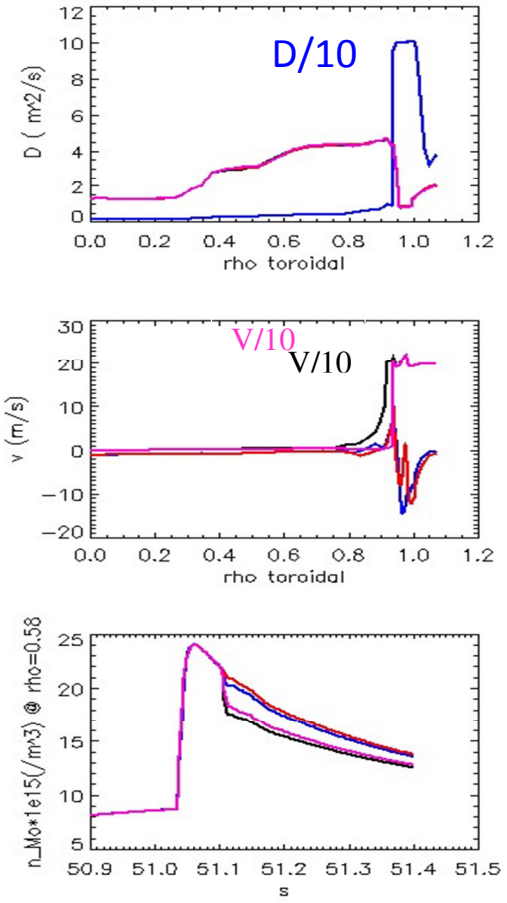

Fig 10. Scan of D and V transport profiles to simulate the ELM and (bottom)impact on the time evolution of Mo density rho=0.6 following the LBO

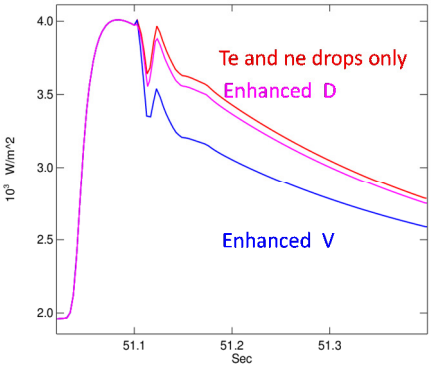

Fig.11. Reconstructed time traces of the SXR Ch T28 in three simulations as labelled.

the black curves of Fig 10, is not dramatically effective. The synthetic chord-integrated SXR traces reproducing Channel 28 of the vertical camera and shown in Fig 11 reflect approximately the drops of Mo density at about mid radius.

4. Summary and conclusions

Trace amounts of Mo, Kr and Ne have been transiently injected into the JET plasma to study in details the way ELM and inter-ELM phases impact on the heavy impurities. The main evidences are that at the level of the ELM amplitude explored, spontaneous and artificial ELMs induced by vertical kicks behave similarly, reducing the density of the injected species by the same amounts when the ELM frequency is comparable. Kr, Ne are affected in a similar way by ELMs, with a content that decreases about linearly with the ELM frequency, for the ELM amplitude explored. The density of tungsten happens to follow closely such dependence. Finally the potential of the LBO technique to study the detailed impact of ELM on impurity transport has been shown. Differences in the way impurities penetrate the plasma because of differences in the pedestal gradients can be observed. In addition, preliminary reconstructions of the signatures left buy the ELMs on the channels of the SXR camera suggest that increasing convection rather than diffusion in the edge barrier region gives better reconstruction s of the experimental evidences. Further work is however needed to make firm statements on the nature of the transport associated to the ELM's.

Acknowledgments

This work has been carried out within the framework of the EUROfusion Consortium and has received funding from the Euratom Research and Training Programme 2014-2018 under grant agreement No 633053. The views and opinions expressed herein do not necessarily reflect those of the European Commission.

References

[1] R NEU et al., Plasma Science, IEEE Transactions on 42, 3 (2014), 552-562,
[2] N FEDORCZAC et al. Journ. Nucl. Mat. 463 (2015).
[3] A LOARTE et al 2014 Nucl. Fusion 54 033007
[4] E de la LUNA et al. Nucl. Fusion **56** 026001, 2016.
[5] P LANG Phys. Plasmas 22, 102501 (2015)
[6] C ANGIONI Phys. Plasmas 22, 102501 (2015)
[7] R DUX et al., IAEA FEC St. Petersburg 2014 paper TH/P3-29
[8] T PUTTERICH, et al., Jour. Nucl. Mat. 415 (2011) S334.
[9] M R WADE et al., Jour Nucl Mat, 337-339 (2005) 737
[10] V PARAIL et al. Journ Nucl. Mat. 463 (2015) 611
[11] R SCANNELL et al., Plasma Phys. Control. Fusion 49 (2007) 1431–1446
[12] T EICH et al 2005 Plasma Phys.Control. Fusion 47 815–42
[13] R MAINGI et al., 2005Nucl. Fusion 45 1066–77
[14] B. KURZAN et al 2005 Phys. Rev. Lett. 95 145001
[15] C SILVA et al., Plasma Phys. Control. Fusion 51(2009) 105001
[16] GTA HUIJSMANS Phys. Plasmas 22, 021805 (2015).
[17] T PUTTERICHet al., IAEA FEC, San Diego EX/P3–15 (2012)
[18] N DEN HARDER et al , Nucl. Fus., 56 (2016) 026014
[19] LAURO TARONI L. et al, Contrib. to Plasma Phys. 32 (1992) 438